LETTER

doi:10.1038/nature13228

The unfolded protein response governs integrity of the haematopoietic stem-cell pool during stress

Peter van Galen[1,2], Antonija Kreso[1,2], Nathan Mbong[1,2], David G. Kent[3], Timothy Fitzmaurice[4], Joseph E. Chambers[5], Stephanie Xie[1,2], Elisa Laurenti[1,2], Karin Hermans[1,2], Kolja Eppert[6], Stefan J. Marciniak[5], Jane C. Goodall[4], Anthony R. Green[3], Bradly G. Wouters[7], Erno Wienholds[1,2] & John E. Dick[1,2]

The blood system is sustained by a pool of haematopoietic stem cells (HSCs) that are long-lived due to their capacity for self-renewal. A consequence of longevity is exposure to stress stimuli including reactive oxygen species (ROS), nutrient fluctuation and DNA damage[1,2]. Damage that occurs within stressed HSCs must be tightly controlled to prevent either loss of function or the clonal persistence of oncogenic mutations that increase the risk of leukaemogenesis[3,4]. Despite the importance of maintaining cell integrity throughout life, how the HSC pool achieves this and how individual HSCs respond to stress remain poorly understood. Many sources of stress cause misfolded protein accumulation in the endoplasmic reticulum (ER), and subsequent activation of the unfolded protein response (UPR) enables the cell to either resolve stress or initiate apoptosis[5,6]. Here we show that human HSCs are predisposed to apoptosis through strong activation of the PERK branch of the UPR after ER stress, whereas closely related progenitors exhibit an adaptive response leading to their survival. Enhanced ER protein folding by overexpression of the co-chaperone ERDJ4 (also called *DNAJB9*) increases HSC repopulation capacity in xenograft assays, linking the UPR to HSC function. Because the UPR is a focal point where different sources of stress converge, our study provides a framework for understanding how stress signalling is coordinated within tissue hierarchies and integrated with stemness. Broadly, these findings reveal that the HSC pool maintains clonal integrity by clearance of individual HSCs after stress to prevent propagation of damaged stem cells.

The human haematopoietic hierarchy has recently been delineated at the single-cell level, enabling precise isolation of HSCs and progenitor cells[7–9] (Extended Data Table 1). Pathway analysis using gene expression signatures from lineage-depleted umbilical cord blood populations revealed enrichment of UPR components in HSCs compared to progenitor cells[10] (Fig. 1a and Extended Data Fig. 1a). The UPR encompasses the IRE1, PERK and ATF6 pathways[6] (Extended Data Fig. 1b). Several genes of the PERK signalling branch were more highly expressed in a mixed population of HSCs and progenitor cells ($CD34^+CD38^-$ HSPCs) compared to downstream progenitors ($CD34^+CD38^+$) isolated from cord blood and adult bone marrow (Fig. 1b and Extended Data Fig. 1c–g). However, splicing of *XBP1* messenger RNA, which is representative of IRE1 activity, was lower in HSPCs compared to progenitors (spliced/total *XBP1*, Fig. 1b). Taken together, gene expression analysis of HSPC and progenitor fractions indicates differential activation of UPR branches, with increased expression of PERK-dependent genes and decreased activity of IRE1 in HSPCs.

To examine whether differential basal UPR gene expression reflects distinct ER stress responses in HSPCs and progenitors, we used two chemical inducers of ER stress: thapsigargin and tunicamycin. Thapsigargin disrupts Ca^{2+} homeostasis in the ER, rapidly activating all three branches of the UPR[11]. Treatment of sorted HSPCs and progenitors with thapsigargin resulted in upregulation of the canonical UPR target genes *GRP94* (also called *HSP90B1*), *GRP78* (*HSPA5*) and *ERDJ4* (Fig. 1c and Extended Data Fig. 2a). *XBP1* mRNA was rapidly spliced in progenitors but to a lesser extent in HSPCs. This indicates that differential *XBP1* splicing between HSPCs and progenitors under steady-state conditions is exaggerated upon thapsigargin-induced ER stress, consistent with repressed IRE1 splicing activity in HSPCs.

Tunicamycin blocks synthesis of N-linked glycoproteins, causing accumulation of unfolded proteins in the ER[11]. Tunicamycin treatment resulted in higher upregulation of the canonical UPR genes *GRP94*, *GRP78* and *ERDJ4* in HSPCs compared to progenitors (Fig. 1d and Extended Data Fig. 2b). Furthermore, upregulation of the PERK pathway constituents *CHOP* (also called *DDIT3*), *ATF4* and *GADD34* (*PPP1R15A*) was higher in HSPCs compared to progenitors. In adult bone marrow, *CHOP* expression was also higher in HSPCs compared to progenitors after addition of a high tunicamycin dose (Extended Data Fig. 2c). Thus, basal enrichment of PERK pathway target genes in HSPCs is further amplified with tunicamycin treatment.

Because persistent ER stress can lead to activation of apoptosis through signals downstream of the IRE1 and PERK branches of the UPR[12], differential UPR branch activation between HSPCs and progenitors might influence cell fate outcome. Thapsigargin treatment did not result in survival differences between HSPCs and progenitors (Extended Data Fig. 3a). However, tunicamycin treatment significantly reduced HSPC viability and clonogenic capacity as compared to progenitors (Fig. 2a–c and Extended Data Fig. 3b, c). Activation of HSPCs into the cell cycle with cytokines reduced the survival difference with progenitors, indicating that tunicamycin sensitivity may be linked to the inherent quiescence of HSPCs (Extended Data Fig. 3d). By focusing on highly purified fractions, we found that tunicamycin caused selective loss by apoptosis of phenotypic $CD34^+CD38^-CD45RA^-CD90^+$ HSCs (Fig. 2d and Extended Data Fig. 3e, f). Overall, these data indicate that tunicamycin-induced ER stress not only elicits distinct UPR signalling in HSCs compared to progenitors, but also causes selective apoptosis of HSCs.

ER stress induces eIF2α phosphorylation (peIF2α) by PERK, leading to global translational attenuation but, paradoxically, ATF4 and CHOP translation is increased[13–15]. ATF4 and CHOP can induce apoptosis following prolonged ER stress, in part by upregulating the eIF2α phosphatase *GADD34*, leading to increased protein load through translational recovery[16,17] (Extended Data Fig. 1b). We investigated whether the increased apoptosis of HSCs compared to progenitors is linked to preferential PERK pathway activation. A lentiviral reporter vector was constructed to measure the ATF4 translation rate[13] (Fig. 3a and Extended Data Fig. 4a–c). As expected, the increased ATF4 reporter activation that occurs after tunicamycin treatment was inhibited by PERK inhibition (measured by transgene ratio, Extended Data Fig. 4d). This activation was more efficient in HSPCs compared to progenitors (Fig. 3b, c),

[1]Princess Margaret Cancer Centre, University Health Network, Toronto, Ontario M5G 2M9, Canada. [2]Department of Molecular Genetics, University of Toronto, Toronto, Ontario M5S 1A8, Canada. [3]Cambridge Institute for Medical Research, Wellcome Trust/MRC Stem Cell Institute and Department of Haematology, University of Cambridge, Cambridge CB2 0XY, UK. [4]Department of Medicine, School of Clinical Medicine, Addenbrookes Hospital, University of Cambridge, Cambridge CB2 0QQ, UK. [5]Cambridge Institute for Medical Research, Wellcome Trust/MRC Stem Cell Institute and Department of Medicine, University of Cambridge, Cambridge CB2 0XY, UK. [6]Department of Pediatrics, McGill University and the Research Institute of the McGill University Health Centre, Westmount, Québec H3Z 2Z3, Canada. [7]Departments of Radiation Oncology and Medical Biophysics, Princess Margaret Cancer Centre, University Health Network, Toronto, Ontario M5G 2M9, Canada.

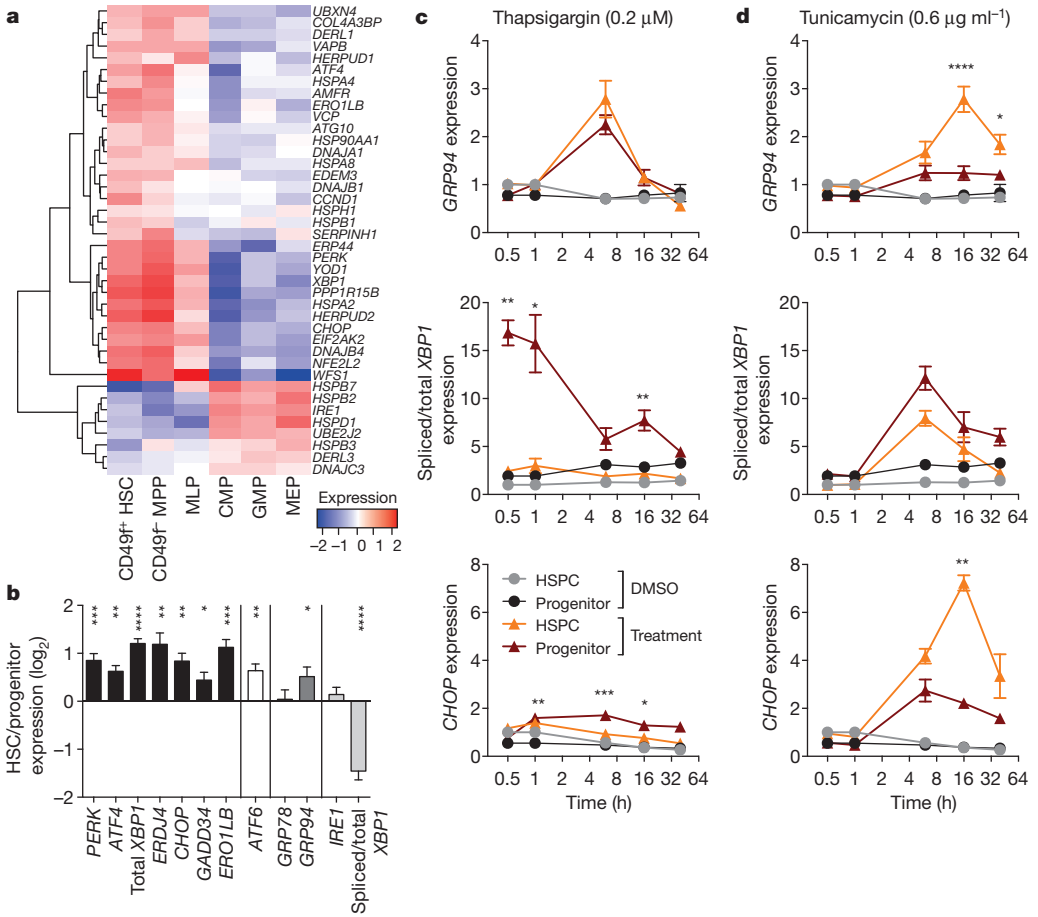

Figure 1 | Elevated expression of PERK branch genes of the UPR in HSCs compared to progenitors and further amplification after tunicamycin-induced stress. **a**, Forty UPR-related genes from the nodes in Extended Data Fig. 1a showed differential expression between HSCs and progenitors (false discovery rate (FDR) <0.05). CMP, common myeloid progenitor; GMP, granulocyte macrophage progenitor; MEP, megakaryocyte erythrocyte progenitor; MPP, multipotent progenitor; MLP, multilymphoid progenitor. **b**, Expression of key UPR genes in HSPC and progenitor fractions was measured by qPCR. Results are shown as mean ± s.e.m. of $n = 6$ cord blood samples. **c**, **d**, UPR branch activation depends on cell type and stressor. Sorted HSPCs or progenitors were plated in the presence of thapsigargin (**c**) or tunicamycin (**d**). RNA was isolated at different time points to measure gene expression by qPCR. DMSO controls were the same between **c** and **d**. Data are shown as mean ± s.e.m. of $n = 3$ cord blood samples; P value was calculated based on treated/control cells and indicates differential response between HSPCs and progenitors. $^*P < 0.05$, $^{**}P < 0.01$, $^{***}P < 0.001$, $^{****}P < 0.0001$.

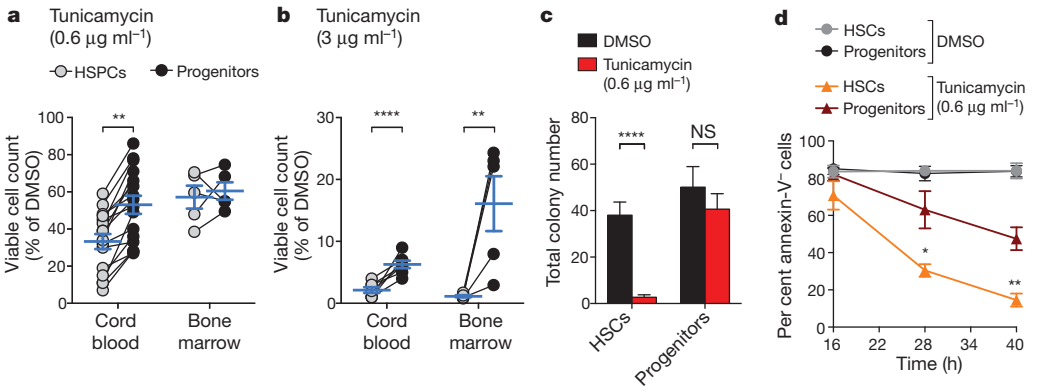

Figure 2 | HSCs are predisposed to apoptosis compared to progenitors after treatment with the ER stress agent tunicamycin. **a**, **b**, Lower survival of cord-blood- and bone-marrow-derived HSPCs compared to progenitors in the presence of tunicamycin. Sorted HSCs/HSPCs and progenitors were plated with 0.6 μg ml^{-1} tunicamycin (**a**) or 3 μg ml^{-1} tunicamycin (**b**). Symbols represent viable cell counts of individual samples where populations are connected by a black line; the blue line indicates mean ± s.e.m. of $n = 16$ cord blood samples and $n = 5$ bone marrow samples (**a**) or $n = 7$ cord blood samples and $n = 5$ bone marrow samples (**b**). **c**, Reduced clonogenic potential of HSCs compared to progenitors following tunicamycin treatment. HSCs or progenitors were sorted into methylcellulose containing DMSO or tunicamycin. Data are shown as mean ± s.e.m. of $n = 4$ cord blood samples; NS, not significant. **d**, Tunicamycin treatment causes higher apoptosis in HSCs compared to progenitors. Cord blood cells were plated with tunicamycin and stained for primitive surface markers and Annexin-V/Sytox. Quantification of viable cells is shown as mean ± s.e.m. of $n = 5$ cord blood samples. P values indicate different viability between HSCs and progenitors. $^*P < 0.05$, $^{**}P < 0.01$, $^{****}P < 0.0001$.

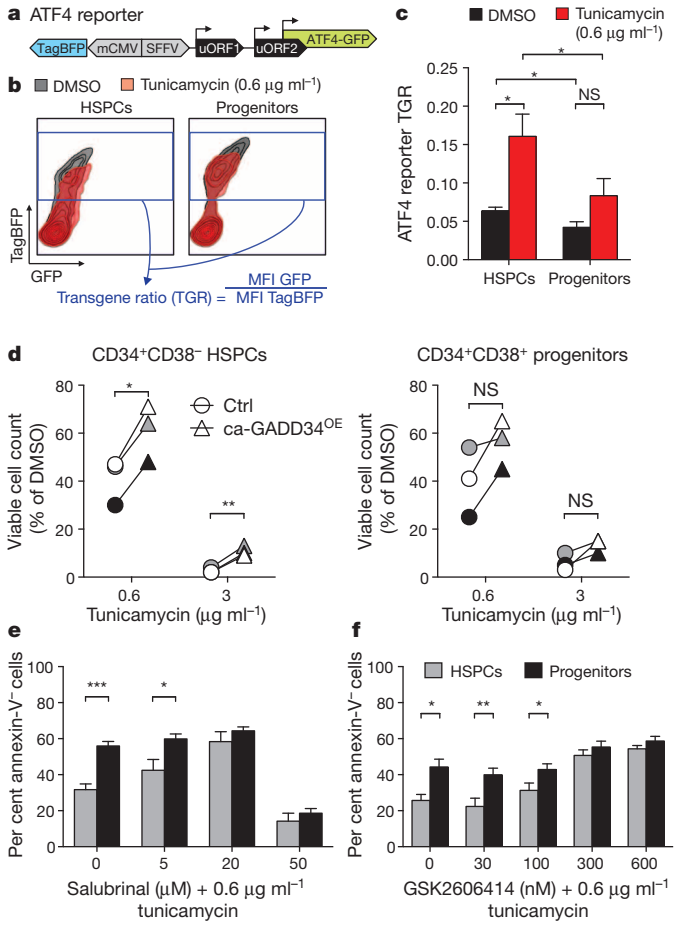

Figure 3 | HSCs are predisposed to UPR-induced apoptosis through PERK–eIF2α–ATF4–CHOP–GADD34 signalling. a, Bidirectional lentiviral reporter vector. All transduced cells are marked by TagBFP; GFP brightness measures the *ATF4* mRNA translation rate, which is regulated by upstream open reading frames (uORFs) and depends on peIF2α (ref. 13). **b**, **c**, Higher ATF4 reporter activity in HSPCs compared to progenitors. HSPCs and progenitors were sorted, transduced with the ATF4 reporter and treated with tunicamycin. **b**, Representative flow plots outline calculation of the transgene ratio. MFI, mean fluorescence intensity. **c**, Results are shown as mean ± s.e.m. of $n = 4$ cord blood samples. **d**, Constitutively active GADD34^{OE} has a more pronounced effect on HSPCs compared to progenitors. Transduced HSPCs (left) or progenitors (right) were treated with tunicamycin. Symbols represent $n = 3$ cord blood samples where control (ctrl) and constitutively active GADD34^{OE} (ca-GADD34^{OE}) groups are connected by a black line; *P* values were calculated using paired *t*-tests. **e**, **f**, Modulating the PERK pathway rescues HSCs from apoptosis. HSPCs and progenitors were plated with tunicamycin and the GADD34 inhibitor salubrinal (**e**) or the PERK inhibitor GSK2606414 (**f**). Viability is shown as mean ± s.e.m. of $n = 5$ (**e**) or $n = 4$ (**f**) cord blood samples. $^*P < 0.05$, $^{**}P < 0.01$, $^{***}P < 0.001$.

indicating that tunicamycin stimulates PERK pathway activity more strongly in HSPCs. As a second method to test PERK pathway involvement, we overexpressed constitutively active GADD34, which prevents peIF2α and upregulation of ATF4 and CHOP[18]. Expression of constitutively active GADD34 significantly increased survival of HSPCs, but not progenitors, after tunicamycin treatment (Fig. 3d). In a third independent approach, HSPCs and progenitors were treated with both tunicamycin and salubrinal, which prevents eIF2α dephosphorylation[19]. Addition of salubrinal preferentially increased HSPC survival after tunicamycin treatment (Fig. 3e). Finally, HSPCs and progenitors were treated with both tunicamycin and the PERK inhibitor GSK2606414 (ref. 20). Like salubrinal, GSK2606414 reduced the survival difference between HSPCs and progenitors (Fig. 3f). Thus, interfering with the PERK pathway at multiple junctions protects HSPCs from tunicamycin-induced apoptosis and equalizes the survival between HSPCs and progenitors. Collectively, these data demonstrate that ER stress preferentially induces apoptosis of HSPCs compared to closely related progenitors through selective activation of the PERK branch of the UPR.

We next asked whether the UPR was involved in regulating HSC function *in vivo*. *CHOP* is a main driver of apoptosis following PERK activation[12,16] and analysis of *Chop*$^{-/-}$ mouse bone marrow showed a small increase in the viability of mouse HSPCs (Extended Data Fig. 5a, b and Extended Data Table 2). This result indicates that *Chop* may be required for the survival/death balance of mouse HSPCs under physiological conditions. Next, we investigated whether enhanced ER protein folding would alter human HSC function. ERDJ4 increases the activity of the chaperone GRP78 and can associate with the ERAD machinery[21,22]. These functions may enhance ER protein folding capacity and protect against UPR-induced apoptosis[23]. *ERDJ4* expression was highest in CD49f^{+} HSCs and reduced in all downstream progenitors (Fig. 4a). Green fluorescent protein (GFP)-marked *ERDJ4* overexpression (ERDJ4^{OE}) lentiviral vectors were constructed to express different transgene levels (Fig. 4b, c). ERDJ4^{OE} conferred protection against tunicamycin-induced cell death in the TEX cell line as well as HSPCs (Fig. 4d and Extended Data Fig. 5c, d), suggesting that ERDJ4^{OE} increases the threshold of ER stress needed to induce apoptosis. To test whether *ERDJ4* influences human HSC function, transduced cord blood cells were transplanted into immune-deficient mice. ERDJ4^{OE} transduced cells had a competitive advantage as compared to the control group (Fig. 4e and Extended Data Fig. 5e). To measure directly the impact of ERDJ4^{OE} on the number of functional HSCs, *in vivo* limiting dilution analysis (LDA) was performed. At a low cell dose, ERDJ4^{OE} resulted in higher engraftment compared to control transduction (Fig. 4f and Extended Data Fig. 5f, g). The LDA measurement demonstrated a 4.4-fold increase in the number of repopulating HSCs on ERDJ4^{OE} (Fig. 4g). These data indicate that a protein folding factor classically associated with the UPR governs HSC function in xenograft assays.

To understand the mechanism of increased human HSC engraftment following ERDJ4^{OE}, we found that ERDJ4^{OE} does not change progenitor engraftment, the frequency of phenotypic stem and progenitor cells, lineage differentiation, homing or self-renewal as measured by secondary LDA (Fig. 4h and Extended Data Fig. 6a–d). We proposed that ERDJ4^{OE} might protect against ER stress that could occur during *in vivo* transplantation. Gene expression analysis of control-transduced cord blood cells indicated increased *CHOP* and *GADD34* expression after transplantation, consistent with a stress response (Fig. 4i). With ERDJ4^{OE}, this surge in *CHOP* and *GADD34* expression was absent, indicating that ERDJ4^{OE} prevents upregulation of stress-related genes. Transplantation of human HSCs in the xenograft environment places them under replicative stress, which causes elevated ROS, DNA damage, and loss of HSC function[2]. These processes may be connected to the UPR as ROS and DNA damage can cause ER stress[5] and ROS accumulation leads to UPR-mediated apoptosis of HSCs[24]. The association between ER protein folding and HSC engraftment indicates that moderation of UPR activation may improve HSC survival during stem-cell transplantation.

Our results establish a previously unrecognized link between UPR signalling and human HSC function. Owing to distinct activation of UPR branches upon stress exposure, HSCs are rapidly cleared while progenitors are spared. This response of human HSCs is consistent with the selective induction of apoptosis after DNA damage or ROS accumulation[2,25]. Collectively, these experimental observations suggest that HSCs possess an intrinsic biological focus on preventing propagation following damage, reducing malignancy risk. Because terminal differentiation purges damaged progenitor cell progeny, clonal purity may be of less importance to progenitors. Loss of HSCs and intestinal stem cells in *Grp78*$^{-/-}$ mice suggests that stem cells of multiple tissues can interrogate ER stress and use differential UPR activation to mitigate against potentially pathological damage[26,27]. Overall, our data point to the elimination of individual

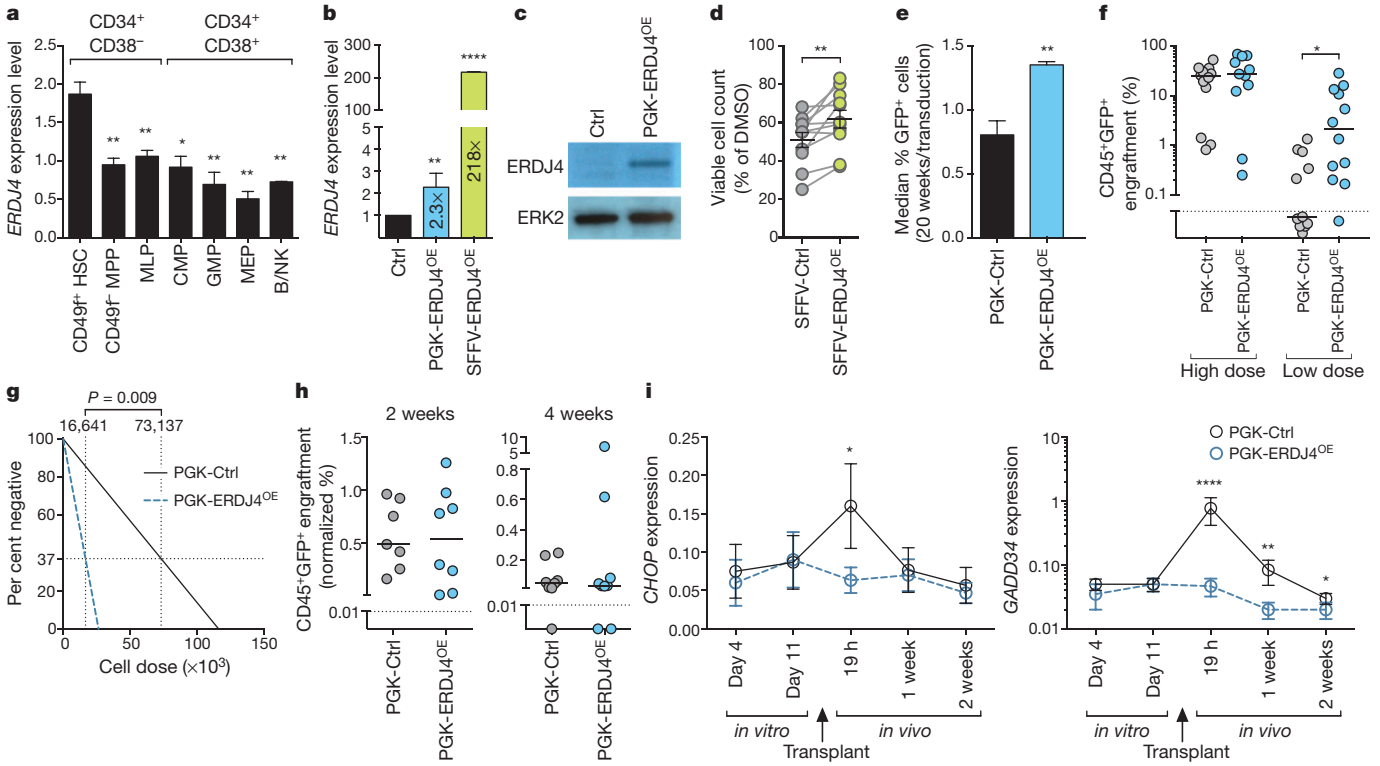

Figure 4 | ERDJ4^{OE} protects from tunicamycin-induced apoptosis and increases HSC output and frequency. **a**, *ERDJ4* expression in sorted cord blood populations (Extended Data Table 1). *P* values were calculated in comparison to CD49f^{+} HSCs; qPCR results are shown as mean ± s.e.m. of $n = 3$ cord blood samples. B/NK, B and NK cell progenitor. **b**, **c**, Validation of lentiviral vectors for ERDJ4^{OE}. **b**, Transduced cord blood cells were analysed by qPCR. PGK and SFFV refer to lentiviral promoter driving *ERDJ4* expression. Results are shown as mean ± s.e.m. of $n = 2$ cord blood samples. **c**, Transduced K562 cells were analysed by western blot. ERK2 is shown as a loading control. **d**, ERDJ4^{OE} protects from tunicamycin-induced apoptosis. Transduced HSPCs were treated with tunicamycin. Symbols represent $n = 11$ cord blood samples where control and ERDJ4^{OE} groups are connected by a grey line; black line indicates mean ± s.e.m.; *P* value was calculated using a paired *t*-test. **e**, ERDJ4^{OE} confers a competitive advantage *in vivo*. Engraftment of transduced cord blood cells was analysed 20 weeks after injection. Data are shown as mean ± s.e.m. of $n = 3$ cord blood samples with 5 mice per group. **f**, **g**, ERDJ4^{OE} increases the number of engrafting HSCs. **f**, Engraftment of transduced cord blood cells was analysed 10 weeks after injection of different cell doses. *P* value was calculated using the Mann–Whitney *U*-test. Every symbol represents one mouse; data represent $n = 3$ cord blood samples with 4 mice per group; line shows median. **g**, HSC frequency was calculated on the basis of the number of engrafted mice. **h**, Progenitors retain normal engraftment capacity with ERDJ4^{OE}. Engraftment of transduced progenitors was assessed 2 and 4 weeks after injection. Data represents $n = 3$ cord blood samples with 3 mice per group; line shows median. **i**, ERDJ4^{OE} moderates a surge in *CHOP* and *GADD34* expression after transplantation. Transduced cord blood cells were expanded *in vitro* and transplanted into mice. *CHOP* and *GADD34* expression in sorted GFP^{+} cells was analysed by qPCR. Data are shown as mean ± s.e.m. of $n = 3$ cord blood samples. $^{*}P < 0.05$, $^{**}P < 0.01$, $^{****}P < 0.0001$.

HSCs after stress and damage as a paradigm of how the stem-cell pool maintains integrity, thereby ensuring long-term tissue maintenance.

METHODS SUMMARY

Umbilical cord blood cells were enriched for CD34^{+} cells and sorted by fluorescence-activated cell sorting (FACS), cultured with small molecules, and/or transduced with lentivirus. Quantitative RT–PCR was performed using primer sequences in Extended Data Table 3. Apoptosis was assessed by Annexin-V/Sytox staining followed by flow cytometry. Human HSC repopulation was read out by intrafemoral transplantation of cord blood cells into immune-deficient mice. Unless otherwise stated, *P* values were calculated by two-tailed unpaired Student's *t*-test.

Online Content Any additional Methods, Extended Data display items and Source Data are available in the online version of the paper; references unique to these sections appear only in the online paper.

Received 25 June 2013; accepted 5 March 2014.
Published online 28 April; corrected online 11 June 2014 (see full-text HTML version for details).

1. Geiger, H., de Haan, G. & Florian, M. C. The ageing haematopoietic stem cell compartment. *Nature Rev. Immunol.* **13,** 376–389 (2013).
2. Yahata, T. *et al.* Accumulation of oxidative DNA damage restricts the self-renewal capacity of human hematopoietic stem cells. *Blood* **118,** 2941–2950 (2011).
3. Shlush, L. I. *et al.* Identification of pre-leukaemic haematopoietic stem cells in acute leukaemia. *Nature* **506,** 328–333 (2014).
4. Rossi, D. J., Jamieson, C. H. M. & Weissman, I. L. Stems cells and the pathways to aging and cancer. *Cell* **132,** 681–696 (2008).
5. Rutkowski, D. T. & Kaufman, R. J. A trip to the ER: coping with stress. *Trends Cell Biol.* **14,** 20–28 (2004).
6. Walter, P. & Ron, D. The unfolded protein response: from stress pathway to homeostatic regulation. *Science* **334,** 1081–1086 (2011).
7. Majeti, R., Park, C. Y. & Weissman, I. L. Identification of a hierarchy of multipotent hematopoietic progenitors in human cord blood. *Cell Stem Cell* **1,** 635–645 (2007).
8. Doulatov, S. *et al.* Revised map of the human progenitor hierarchy shows the origin of macrophages and dendritic cells in early lymphoid development. *Nature Immunol.* **11,** 585–593 (2010).
9. Notta, F. *et al.* Isolation of single human hematopoietic stem cells capable of long-term multilineage engraftment. *Science* **333,** 218–221 (2011).
10. Laurenti, E. *et al.* The transcriptional architecture of early human hematopoiesis identifies multilevel control of lymphoid commitment. *Nature Immunol.* **14,** 756–763 (2013).
11. DuRose, J. B., Tam, A. B. & Niwa, M. Intrinsic capacities of molecular sensors of the unfolded protein response to sense alternate forms of endoplasmic reticulum stress. *Mol. Biol. Cell* **17,** 3095–3107 (2006).
12. Tabas, I. & Ron, D. Integrating the mechanisms of apoptosis induced by endoplasmic reticulum stress. *Nature Cell Biol.* **13,** 184–190 (2011).
13. Lu, P. D., Harding, H. P. & Ron, D. Translation reinitiation at alternative open reading frames regulates gene expression in an integrated stress response. *J. Cell Biol.* **167,** 27–33 (2004).
14. Vattem, K. M. & Wek, R. C. Reinitiation involving upstream ORFs regulates ATF4 mRNA translation in mammalian cells. *Proc. Natl Acad. Sci. USA* **101,** 11269–11274 (2004).
15. Palam, L. R., Baird, T. D. & Wek, R. C. Phosphorylation of eIF2 facilitates ribosomal bypass of an inhibitory upstream ORF to enhance CHOP translation. *J. Biol. Chem.* **286,** 10939–10949 (2011).

16. Marciniak, S. J. *et al.* CHOP induces death by promoting protein synthesis and oxidation in the stressed endoplasmic reticulum. *Genes Dev.* **18,** 3066–3077 (2004).
17. Han, J. *et al.* ER-stress-induced transcriptional regulation increases protein synthesis leading to cell death. *Nature Cell Biol.* **15,** 481–490 (2013).
18. Novoa, I., Zeng, H., Harding, H. P. & Ron, D. Feedback inhibition of the unfolded protein response by GADD34-mediated dephosphorylation of eIF2α. *J. Cell Biol.* **153,** 1011–1022 (2001).
19. Boyce, M. *et al.* A selective inhibitor of eIF2α dephosphorylation protects cells from ER stress. *Science* **307,** 935–939 (2005).
20. Axten, J. M. *et al.* Discovery of 7-methyl-5-(1-{[3-(trifluoromethyl)phenyl]acetyl}-2,3-dihydro-1H-indol-5-yl)-7H-pyrrolo[2,3-d]pyrimidin-4-amine (GSK2606414), a potent and selective first-in-class inhibitor of protein kinase R (PKR)-like endoplasmic reticulum kinase (PERK). *J. Med. Chem.* **55,** 7193–7207 (2012).
21. Shen, Y., Meunier, L. & Hendershot, L. M. Identification and characterization of a novel endoplasmic reticulum (ER) DnaJ homologue, which stimulates ATPase activity of BiP *in vitro* and is induced by ER stress. *J. Biol. Chem.* **277,** 15947–15956 (2002).
22. Lai, C. W., Otero, J. H., Hendershot, L. M. & Snapp, E. ERdj4 protein is a soluble endoplasmic reticulum (ER) DnaJ family protein that interacts with ER-associated degradation machinery. *J. Biol. Chem.* **287,** 7969–7978 (2012).
23. Kurisu, J. *et al.* MDG1/ERdj4, an ER-resident DnaJ family member, suppresses cell death induced by ER stress. *Genes Cells* **8,** 189–202 (2003).
24. Rouault-Pierre, K. *et al.* HIF-2α protects human hematopoietic stem/progenitors and acute myeloid leukemic cells from apoptosis induced by endoplasmic reticulum stress. *Cell Stem Cell* **13,** 549–563 (2013).
25. Milyavsky, M. *et al.* A distinctive DNA damage response in human hematopoietic Stem cells reveals an apoptosis-independent role for p53 in self-renewal. *Cell Stem Cell* **7,** 186–197 (2010).
26. Heijmans, J. *et al.* ER stress causes rapid loss of intestinal epithelial stemness through activation of the unfolded protein response. *Cell Rep.* **3,** 1128–1139 (2013).
27. Wey, S., Luo, B. & Lee, A. S. Acute inducible ablation of GRP78 reveals its role in hematopoietic stem cell survival, lymphogenesis and regulation of stress signaling. *PLoS ONE* **7,** e39047 (2012).

Acknowledgements We thank D. Ron and D. Rubinsztein for critical assessment of this work; all members of the Dick laboratory, especially O. I. Gan and E. Lechman, for experimental support and advice; A. Khandani, P. Penttilä and the SickKids-UHN flow facility for technical support; N. Jamal for providing bone marrow samples; J. Heijmans for providing the pLV-ca-GADD34 vector; and L. Naldini for providing the MA1 vector. Work in the Dick laboratory is supported by grants from the Canadian Institutes for Health Research, Canadian Cancer Society, Terry Fox Foundation, Genome Canada through the Ontario Genomics Institute, Ontario Institute for Cancer Research with funds from the province of Ontario, a Canada Research Chair and the Ontario Ministry of Health and Long Term Care (OMOHLTC). The views expressed do not necessarily reflect those of the OMOHLTC. A.R.G. and D.G.K. are supported by Leukemia and Lymphoma Research, Cancer Research UK, the Kay Kendall Leukaemia Fund, the NIHR Cambridge Biomedical Research Centre, the Cambridge Experimental Cancer Medicine Centre, and the Leukemia & Lymphoma Society of America. J.C.G. and T.F. are supported by Arthritis Research UK. S.J.M. and J.E.C. are supported by the Medical Research Council (UK). B.G.W. is supported by the Terry Fox New Frontiers Research Program (PPG09-020005), the Ontario Institute for Cancer Research, and the Canadian Institute for Health Research (CIHR grant 201592).

Author Contributions P.v.G., A.K. and J.E.D. designed the study and analysed and interpreted the data. P.v.G., A.K., N.M., D.G.K., T.F., J.E.C., S.X., K.H. and E.W. performed experiments. E.L. and K.E. performed bioinformatic analyses. S.J.M., J.C.G., A.R.G. and B.G.W. supervised specific experiments. P.v.G. wrote the paper. A.K. and J.E.D. revised the paper. J.E.D. supervised the study.

Author Information Reprints and permissions information is available at www.nature.com/reprints. The authors declare no competing financial interests. Readers are welcome to comment on the online version of the paper. Correspondence and requests for materials should be addressed to J.E.D. (jdick@uhnresearch.ca).

METHODS

Cord blood and bone marrow sample preparation and liquid cell culture. Umbilical cord blood, bone marrow or mobilized peripheral blood from healthy individuals was obtained with informed consent according to procedures approved by the institutional review boards of the University Health Network and Trillium Hospital. Mononuclear cells were obtained by centrifugation on Ficoll, and lineage depletion was performed using the StemSep Human Progenitor Cell Enrichment Kit according to the manufacturer's protocol (50–75% $CD34^+$, StemCell Technologies). The Lin^- cord blood or Lin^- bone marrow/mobilized peripheral blood cells were stored in IMDM with 50% FCS and 10% DMSO at −150 °C until use. Unless stated otherwise, HSC/HSPC and progenitor fractions were sorted from cord blood. For liquid culture, cells were thawed and plated in X-VIVO 10 (BioWhittaker) supplemented with 1% BSA, 2 mM L-glutamine, 100 U ml^{-1} penicillin-streptomycin, and the following cytokines: TPO (7.5 ng ml^{-1}), SCF (50 ng ml^{-1}), G-CSF (5 ng ml^{-1}), Flt3 ligand (50 ng ml^{-1}) and IL-6 (5 ng ml^{-1}), referred to as TSGF6 culture. The cell line K562 was expanded in IMDM with 10% FCS, 2 mM L-glutamine and 100 U ml^{-1} penicillin-streptomycin; TEX cells were cultured as reported previously[28]. Both cell lines tested negative for mycoplasma.

Fluorescence-activated cell sorting and flow cytometry. To separate cell populations, cord blood or bone marrow cells were re-suspended at 10^7 cells per ml, stained with antibodies against surface markers in PBS with 2% FCS, washed and sorted on the BD FACS Aria or MoFlo, consistently yielding >95% purity. Analytical flow cytometry was performed using BD LSRII or BD Canto cytometer. Data was analysed with FlowJo software (Tree Star, Inc.).

Annexin-V/Sytox and cleaved caspase-3 flow cytometry. For Annexin-V/Sytox apoptosis analysis, cells were stained for surface markers and washed in PBS with 2% FCS, re-suspended in binding buffer (diluted 10 × in H_2O, BD catalogue number 556454) with Annexin-V-APC (50 × dilution, BD 550474) and Sytox Blue (500 × dilution, Life Technologies S34857) and stained for 20 min at room temperature. Then the sample was diluted 5× with binding buffer and cells were analysed by flow cytometry within 60 min. For cleaved caspase-3 analysis, cells were permeabilized for 30 min at room temperature with BD Perm 2 buffer (diluted 10 × in H_2O, catalogue number 347692), washed in 2 ml PBS with 2% FCS and stained with PE-conjugated cleaved caspase-3 antibody from BD (catalogue number 561011) for 30 min at room temperature. Cells were washed again and re-suspended in BD Cytofix buffer (diluted 4 × in PBS, BD catalogue number 554655) before flow cytometry analysis.

Quantitative RT–PCR. RNA was extracted from 500–100,000 cells using TRIzol (Life Technologies) and re-suspended in water for cDNA synthesis using the SuperScript III or SuperScript VILO systems according to manufacturer's instructions (Life Technologies). For each qPCR reaction we added 2 × Power SYBR Green mix (Life Technologies), 133 nM forward primer and 133 nM reverse primer and RNase-free water up to a total volume of 12.5 µl. cDNA was diluted 6–20× with RNase-free water and 2.5 µl was added for each reaction. The qPCR was performed using a 7900 HT Real-Time PCR system with SDS v2.3 software (Applied Biosystems) using standard settings: 50 °C for 2 min; 95 °C for 10 min; then 95 °C for 15 s and 60 °C for 1 min repeated for 40 cycles; then dissociation stage. Each assay was run in duplicate for technical variation. Arbitrary mRNA concentrations were calculated using the relative standard curve method. Gene expression levels were normalized to *GAPDH* except in Fig. 1b (normalized to the average of *GAPDH*, *ACTB* and *PBGD*) and Fig. 4a (normalized to the average of *GAPDH* and *ACTB*). To determine *XBP1* splicing levels, primers were designed that amplify all or only spliced *XBP1* mRNA, and spliced *XBP1* expression was divided by total *XBP1* expression (indicated as spliced/total *XBP1*). qPCR primer sequences are listed in Extended Data Table 3.

Methylcellulose colony-forming assays. Methylcellulose (StemCell Technologies MethoCult H4034) was supplemented with IL-6 (10 ng ml^{-1}), Flt3 ligand (10 ng ml^{-1}) and DMSO or tunicamycin (0.6 µg ml^{-1}). Using the BD FACS Aria, 500 $CD34^+$ $CD38^-CD45RA^-CD90^+$ HSCs or 350 $CD34^+CD38^+$ progenitors were deposited in 2.5 ml methylcellulose, and duplicate dishes were plated with 1 ml each (200 HSCs or 140 progenitors per dish). After 13 days, colonies were counted and classified based on morphological appearance.

Lentiviral vectors. The bidirectional lentiviral MA1 vector[29] was modified by replacing ΔNGFR with a *loxP*-flanked Gateway cassette (Life Technologies) to generate the destination vector pMAL. To generate PGK-ERDJ4^{OE}, pMAL was recombined with the *ERDJ4* entry vector from the Mammalian Gene Collection through the PlasmID Repository at Harvard[30] (Clone ID HsCD00076069). To generate constitutively active (ca) GADD34^{OE}, the *GADD34* fragment was amplified by PCR from the pLV-ca-GADD34 construct[26] using the forward primer 5′-CACCATGGCCA GTGTGCTGG-3′ and the reverse primer 5′-TCACTGGGAAGGGAAGAAGG-3′, cloned into an entry vector using the pENTR Directional TOPO cloning kit (Life Technologies K2400-20), and this entry vector was recombined with pMAL. To generate SFFV-ERDJ4^{OE}, the PGK promoter of PGK-ERDJ4^{OE} was replaced with the stronger SFFV promoter[31]. Control (Ctrl) vectors expressed a humanized *Renilla* luciferase gene or a Stuffer sequence derived from pLKO.1_1.9Kb_stuffer instead of *ERDJ4* and *ca-GADD34*. The ATF4 reporter lentivirus was made as follows: first, the PGK promoter in pMAL was replaced with the stronger SFFV promoter and GFP was replaced with TagBFP (Evrogen[32]) to generate the destination vector pSMALB. Next, the reporter fragments were amplified from ATF4.5: 5′ATF4.GFP (Addgene 21852), ATF4.12: 5′ATF4.uORF1^{AUA}.GFP (Addgene 21859) and ATF4.14: 5′ATF4.uORF1&2^{AUA}.GFP (Addgene 21861) using the forward primer 5′-C ACCAGCTTTTCTGCTTGCTGTC-3′ and the reverse primer 5′-TTACTTGTA CAGCTCGTC CATGC-3′. These fragments were cloned into entry vectors using the pENTR Directional TOPO cloning kit. Finally, the entry vectors were recombined with pSMALB to generate the bidirectional lentiviral reporter vectors pSMALB-ATF4.5rep (referred to as ATF4 reporter), pSMALB-ATF4.12rep and pSMALB-ATF4.14rep, respectively. In the ATF4 reporter, mRNA expression highly correlates between TagBFP and ATF4–GFP due to the bidirectional promoter[29]. To account for differences in basal translation between experimental conditions (such as HSPCs versus progenitors, high versus low transduction, DMSO versus tunicamycin treatment), we calculated the transgene ratio between GFP and TagBFP as a measure of reporter activity (TGR = GFP mean fluorescence intensity/TagBFP mean fluorescence intensity, Fig. 3b). Reporter fluorescence was measured 30 h after addition of tunicamycin. For *in vitro* experiments, transduced cord blood cells were cultured for 3 days before treatment to allow for gene expression to come up.

Lentivirus production and primary cell transduction. Viral particles were pseudotyped with the vesicular stomatitis virus G (VSVG) protein using the pMD.G vector and third-generation pMDLg/pRRE and pRSVRev vectors were used for packaging in 293T cells using calcium-phosphate transfection (Clontech catalogue number 631312). Lentivirus was concentrated 100× by ultracentrifugation, resuspended in X-VIVO 10 (BioWhittaker) supplemented with 1% BSA and stored at –80 °C until use. Cord blood cells were thawed and plated in liquid TSGF6 culture with double the concentration of all cytokines, and lentiviral suspension was added at a multiplicity of infection of 5–20 in a total volume of 100 µl (96 well plate) or 400 µl (24 well plate). After 16 h, TSGF6 culture medium was added to expand the cells. Transduction was measured using flow cytometry for GFP or TagBFP after 72–96 h.

Mouse xenotransplantation and human Lin^- cell isolation. Mouse xenografts were performed as described previously[33] according to protocols approved by the University Health Network Animal Care Committee. Briefly, 8–12-week-old male NOD/Lt-scid/IL2Rγnull (NSG) mice were sublethally irradiated (225 cGy) 1 day before injection. Cells were injected intrafemorally with 30 µl PBS. Peripheral blood (80 µl) was taken from the saphenous vein and analysed by flow cytometry. Mice with >40% human T cells in the peripheral blood are likely to harbour an autoimmune clonal T-cell expansion and were excluded from analysis. To reach statistical significance, all animal studies were repeated with 3 cord blood samples with at least 2, but generally 5, mice per condition. Animals were not randomized before injection, no blinding was done for animal studies. After the mice were euthanized, femurs were flushed with 2 ml PBS 2% FCS; 50 µl was stained for surface markers and analysed by flow cytometry. Unless stated otherwise, engraftment data for injected femur is shown. For lineage depletion, bone marrow cells from the femurs and tibias of 5 mice were combined and processed with the StemSep Mouse/Human Chimera Enrichment kit (Stem Cell Technologies) according to the manufacturer's instructions. However, during the antibiotin incubation step, an additional 50 µl ml^{-1} human haematopoietic progenitor enrichment antibody cocktail from the StemSep Human Progenitor Cell Enrichment Kit was added to deplete human lineage-positive cells.

***In vivo* repopulation and serial limiting dilution analysis.** For competitive repopulation experiments, cord blood cells were transduced and ~50,000 cells were injected per mouse the next day. After 20 weeks, the mouse bone marrow was analysed for human $CD45^+$ engraftment as well as GFP and lineage differentiation. The median percentage of GFP^+ cells within the human $CD45^+$ graft was normalized to initial transduction for PGK-Ctrl and PGK-ERDJ4^{OE} groups. For limiting dilution analysis (LDA) in primary recipients, transduced cord blood cells were expanded for 10 days in liquid TSGF6 culture and GFP^+ cells were sorted and injected at low and high cell doses. Human $CD45^+GFP^+$ engraftment was analysed 10 weeks after transplantation. LDA in secondary recipient mice was performed by sorting GFP^+ cells from pooled bone marrow of primary mice. Secondary mice were injected with 30,000 to 1,000,000 cells and analysed 10 weeks after transplantation; a secondary mouse was scored as positive if it had >0.01% human engraftment. HSC frequency was estimated using the ELDA software[34] (Extreme Limiting Dilution Analysis, http://bioinf.wehi.edu.au/software/elda/). Progenitor engraftment was tested by overnight transduction of sorted $CD34^+CD38^+$ progenitors and injection of 8,700–14,000 cells per mouse. The percentage of human $CD45^+GFP^+$ cells in the mouse bone marrow after 2–4 weeks was normalized to initial transduction. To assess gene expression changes on transplantation, mice were killed at 19 h, 1 week and 2 weeks after transplantation of 1.0–1.6 × 10^6 transduced cord blood

cells. Human GFP^+CD34^+ cells were sorted from the xenografted mouse bone marrow (at 19 h and 1 week after transplant, all GFP^+ cells were sorted due to cell number constraints).

Analysis of *Chop*$^{-/-}$ mouse bone marrow. *Chop*$^{-/-}$ and wild-type littermates on the C57BL/6 background were housed in a specific pathogen-free facility according to the Animals Scientific Procedures outlined by the UK. Femurs, tibias and pelvises of 13-week-old male mice were flushed to isolate bone marrow cells. Five to ten million cells were stained with antibodies against surface markers (HSC panel: lineage markers, c-Kit, Sca-1, CD34 and Flk2; progenitor panel: lineage markers, c-Kit, Sca-1, CD34 and FcγII/IIIR, Extended Data Table 2). Next, cells were stained using Annexin-V Pacific Blue conjugate (Biolegend) and 7-AAD according to manufacturer's instructions, and analysed on a BD Fortessa cytometer.

Tunicamycin, thapsigargin, salubrinal and GSK2606414. Compounds were purchased as follows: tunicamycin, Sigma-Aldrich, catalogue number T7765; thapsigargin, Sigma-Aldrich, catalogue number T9033; salubrinal, Santa Cruz, catalogue number SC202332; GSK2606414, Merck Millipore, catalogue number 516535. Powder was re-suspended in DMSO and stored at −20 °C until use. Final DMSO concentration was always <0.6% and equal between treatment and control groups. Unless otherwise indicated, cell counts and viability analyses were performed after 40 h of treatment. Viable cells were counted manually by Trypan blue exclusion or automated using the BD Canto flow cytometer high throughput sampler (HTS), by counting the number of $Annexin^-$ and/or $Sytox^-$ cells in a specified volume.

Western blot. Transduced K562 cells were lysed, separated with SDS–PAGE and transferred onto a polyvinylidene fluoride membrane as previously reported[33]. Specific antibody to ERDJ4 (Abnova catalogue number H00004189-M09) was detected using secondary HRP-conjugated antibodies (Amersham) and visualized by chemiluminescence (Pierce).

Gene expression and pathway analysis. Gene expression data sets were reported previously[10]. The genes upregulated in HSC compared to progenitor (MLP/CMP/GMP/MEP) with adjusted *P* value <0.01 were used for gene ontology (GO) analyses with BiNGO[35]. The algorithm was used with hypergeometric test, multiple test correction (Benjamini–Hochberg false discovery rate (FDR)) and using the whole *Homo sapiens* annotation as a reference set. Data were visualized with Cytoscape[36]; gene sets linked to the UPR response were unlinked from the rest of the network for presentation. For the heat map, we checked the expression of all genes belonging to GO categories relative to the UPR response (79 genes belonging to GO_0006986, GO_0034620, GO_0034976, GO_0030968 categories). Forty of these were differentially expressed between HSC and progenitors (FDR <0.05). Their expression levels in HSC, MPP, MLP, CMP, GMP and MEP were mean centred.

Statistical analysis. Unless otherwise stated, mean ± s.e.m. values are given and *P* values were calculated by two-tailed unpaired Student's *t*-test. Mann–Whitney *U*-tests were performed to compare engraftment levels, as these data do not show a normal distribution. ELDA software was used for statistical analysis of *in vivo* LDA[34] (http://bioinf.wehi.edu.au/software/elda). $*P < 0.05$, $**P < 0.01$, $***P < 0.001$, $****P < 0.0001$.

28. Warner, J. K. *et al.* Direct evidence for cooperating genetic events in the leukemic transformation of normal human hematopoietic cells. *Leukemia* **19,** 1794–1805 (2005).
29. Amendola, M., Venneri, M. A., Biffi, A., Vigna, E. & Naldini, L. Coordinate dual-gene transgenesis by lentiviral vectors carrying synthetic bidirectional promoters. *Nature Biotechnol.* **23,** 108–116 (2005).
30. The MGC Project Team. The status, quality, and expansion of the NIH full-length cDNA project: the Mammalian Gene Collection (MGC). *Genome Res.* **14,** 2121–2127 (2004).
31. Gentner, B. *et al.* Stable knockdown of microRNA *in vivo* by lentiviral vectors. *Nature Methods* **6,** 63–66 (2009).
32. Subach, O. M. *et al.* Conversion of red fluorescent protein into a bright blue probe. *Chem. Biol.* **15,** 1116–1124 (2008).
33. van Galen, P. *et al.* Reduced lymphoid lineage priming promotes human hematopoietic stem cell expansion. *Cell Stem Cell* **14,** 94–106 (2014).
34. Hu, Y. & Smyth, G. K. ELDA: extreme limiting dilution analysis for comparing depleted and enriched populations in stem cell and other assays. *J. Immunol. Methods* **347,** 70–78 (2009).
35. Maere, S., Heymans, K. & Kuiper, M. BiNGO: a Cytoscape plugin to assess overrepresentation of gene ontology categories in biological networks. *Bioinformatics* **21,** 3448–3449 (2005).
36. Lopes, C. T. *et al.* Cytoscape Web: an interactive web-based network browser. *Bioinformatics* **26,** 2347–2348 (2010).
37. Yoshida, H., Matsui, T., Yamamoto, A., Okada, T. & Mori, K. XBP1 mRNA is induced by ATF6 and spliced by IRE1 in response to ER stress to produce a highly active transcription factor. *Cell* **107,** 881–891 (2001).
38. Lin, J. H. *et al.* IRE1 signaling affects cell fate during the unfolded protein response. *Science* **318,** 944–949 (2007).
39. Harding, H. P., Zhang, Y. & Ron, D. Protein translation and folding are coupled by an endoplasmic-reticulum-resident kinase. *Nature* **397,** 271–274 (1999).

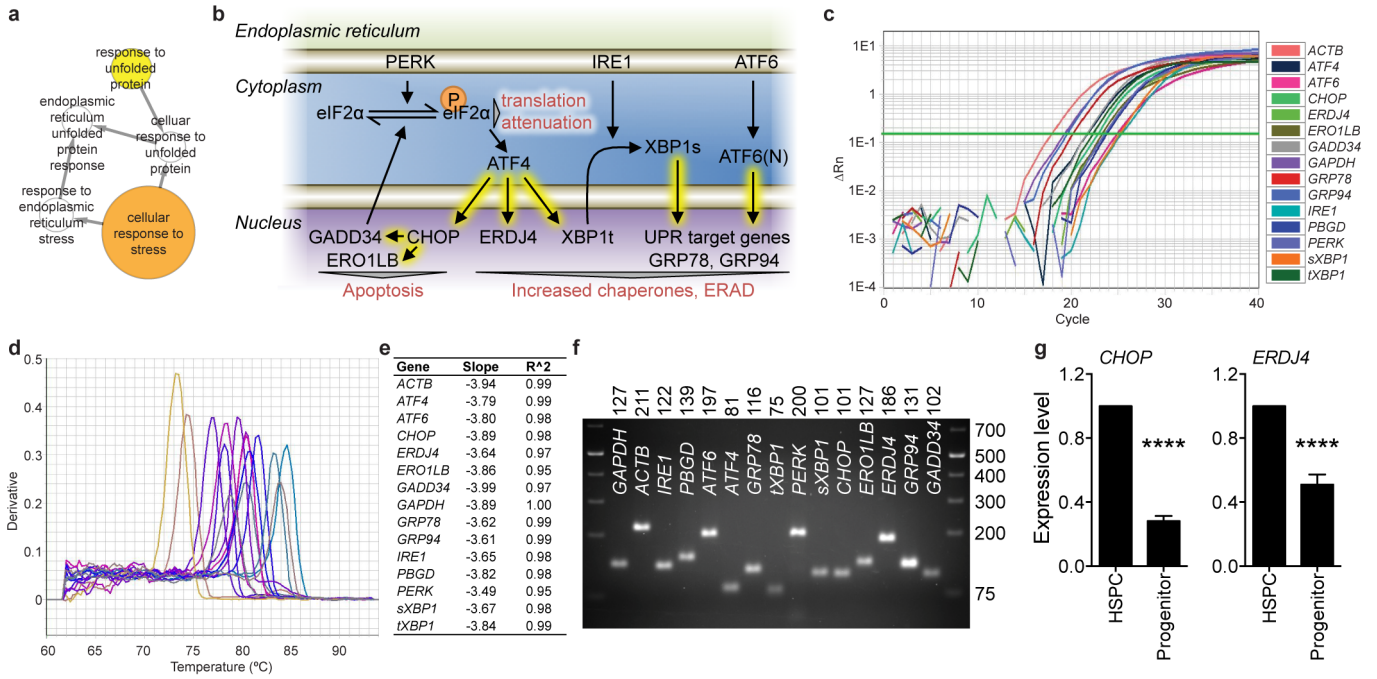

Gene	Slope	R^2
ACTB	-3.94	0.99
ATF4	-3.79	0.99
ATF6	-3.80	0.98
CHOP	-3.89	0.98
ERDJ4	-3.64	0.97
ERO1LB	-3.86	0.95
GADD34	-3.99	0.97
GAPDH	-3.89	1.00
GRP78	-3.62	0.99
GRP94	-3.61	0.99
IRE1	-3.65	0.98
PBGD	-3.82	0.98
PERK	-3.49	0.95
sXBP1	-3.67	0.98
tXBP1	-3.84	0.99

Extended Data Figure 1 | Expression analysis of UPR-related genes. **a**, Enrichment of UPR-related genes in human HSCs compared to progenitors. CD49f^{+} HSC-enriched genes were analysed for GO category overrepresentation. Node size represents the number of genes; white, yellow and orange colour correspond to FDR <0.15, <0.1 and <0.01. **b**, Simplified scheme illustrating UPR signalling events. Three branches of the UPR are activated upon ER stress: IRE1, PERK and ATF6. IRE1 splices cytosolic *XBP1* mRNA to enable translation of the XBP1s transcription factor, which upregulates chaperones and ER-associated degradation (ERAD) machinery to resolve ER stress[37,38]. PERK initiates a different branch of the UPR through phosphorylation of eIF2α, which attenuates global protein synthesis, thus permitting time to restore ER homeostasis[39]. Prolonged ER stress leads to PERK signalling-mediated upregulation of the proapoptotic transcription factor *CHOP* and its target *GADD34.* GADD34 dephosphorylates eIF2α leading to restoration of global protein translation. However, if ER stress is not resolved, *GADD34* upregulation can lead to further accumulation of misfolded proteins, oxidative stress and apoptosis[16]. Yellow highlighted arrows indicate transcriptional regulation. **c**, Amplification curves of qPCR reactions for UPR-related genes. Fluorescence signal during 40 cycles of qPCR reactions on cord-blood-derived cDNA is shown for a representative experiment. Green line indicates threshold that was used to calculate mRNA quantity. **d**, Dissociation curves were generated to check for the presence of aspecific amplicons or primer dimers, which would be visible as additional peaks. Each line represents the dissociation curve of one qPCR reaction, colours indicate different genes. **e**, Slopes and R^2 values of standard curves are shown for a representative experiment. These values were calculated separately for each experiment, based on a cDNA dilution series. **c**–**e** were performed using SDS v2.3 software. **f**, Agarose gel analysis of qPCR amplicons. qPCR reactions were run on a 3% agarose gel to check for reaction specificity: nonspecific amplicons would be visible as additional bands. The expected product size is shown above the gel; the ladder sizes are indicated on the right. **g**, Adult bone marrow cells were sorted into HSPC and progenitor fractions. mRNA levels for *CHOP* and *ERDJ4* were measured by qPCR. Results are shown as mean ± s.e.m. of $n = 5$ bone marrow samples. ****$P < 0.0001$.

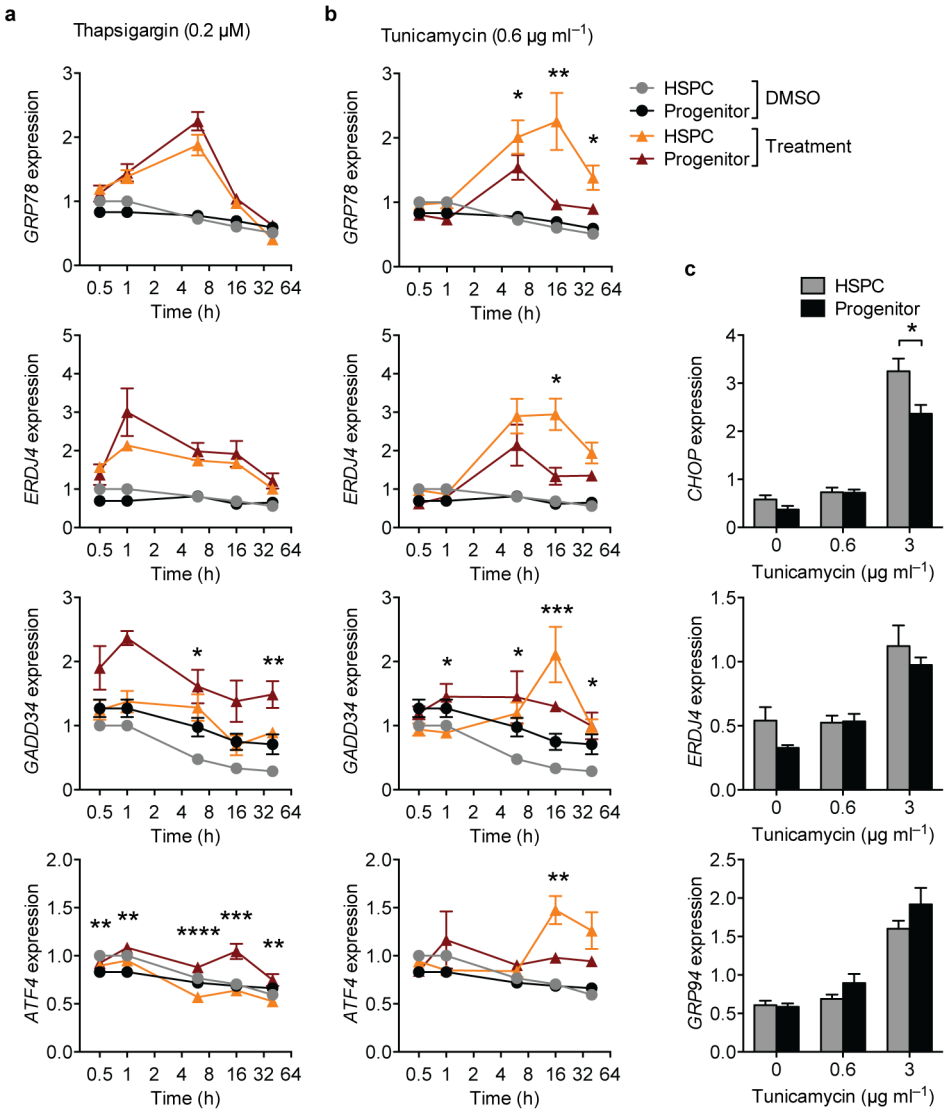

Extended Data Figure 2 | Differential response of HSPCs and progenitors to ER-stress-inducing agents. **a**, **b**, HSPC and progenitor fractions were sorted and plated in the presence of (**a**) thapsigargin or (**b**) tunicamycin. mRNA was isolated after 0.5, 1, 6, 16 and 40 h and expression levels of *GRP78*, *ERDJ4*, *GADD34* and *ATF4* were assessed by qPCR. The DMSO-treated controls were the same between **a** and **b**. Data are shown as mean ± s.e.m. of $n = 3$ cord blood samples, *P* value was calculated based on fold change of treated over DMSO control cells and indicates differential response between HSPCs and progenitors. **c**, Adult bone marrow HSPCs and progenitors were sorted and plated in the presence of tunicamycin. After 16 h, mRNA was isolated and expression levels of *CHOP*, *ERDJ4* and *GRP94* were assessed by qPCR. Data are shown as mean ± s.e.m. of $n = 5$ bone marrow samples.

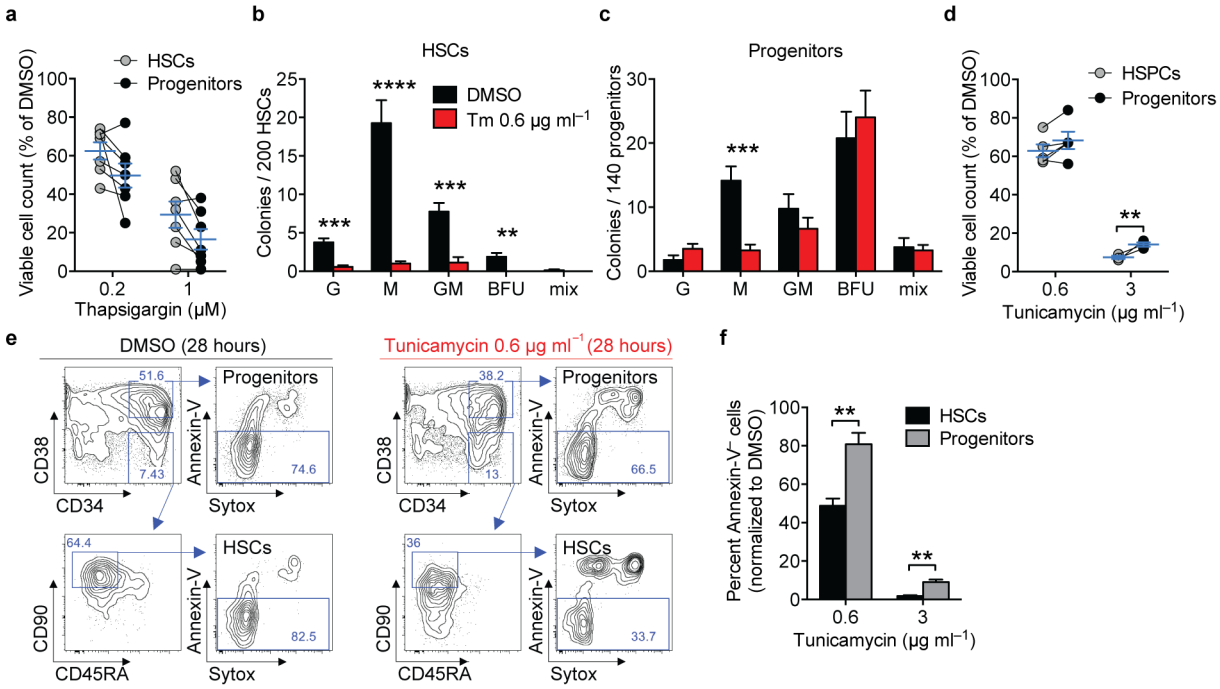

Extended Data Figure 3 | Survival of HSCs is lower compared to progenitors after tunicamycin, but not thapsigargin treatment. **a**, Thapsigargin has similar toxicity for sorted HSC and progenitor fractions. Sorted HSCs and progenitors were plated in TSGF6 culture conditions in the presence of thapsigargin or DMSO control. Symbols represent viable cell counts of individual samples where fractions are connected by a black line; the blue line indicates mean ± s.e.m. of $n = 7$ cord blood samples. **b**, **c**, Reduced clonogenic capacity of sorted HSCs compared to progenitors after tunicamycin treatment. Total colony number is shown in Fig. 2c. Here, data are separated into colony types based on morphological appearance. Data are shown as mean ± s.e.m. of $n = 4$ cord blood samples. G, granulocyte; M, macrophage; GM, granulocyte/macrophage; BFU, erythroid burst forming unit; mix, multilineage. **d**, HSCs have lower survival compared to progenitors after tunicamycin treatment, even after cell cycle induction. Sorted HSC and progenitor fractions were plated in TSGF6 culture conditions with double cytokine concentrations for 72–96 h to induce G0 exit of the HSC fraction[33]. Then, cells were plated in the presence of tunicamycin. Viable cell counts as a percentage of DMSO controls are shown. Symbols represent individual samples where fractions are connected by a black line; the blue line indicates mean ± s.e.m. of $n = 5$ cord blood samples at 0.6 μg ml^{-1} and $n = 3$ cord blood samples at 3 μg ml^{-1} tunicamycin. **e**, **f**, Increased apoptosis of HSCs compared to progenitors after tunicamycin treatment. **e**, Cord blood cells were plated with tunicamycin and stained for primitive surface markers, Annexin-V and Sytox. Representative flow plots are shown. **f**, Sorted HSCs and progenitors were plated in the presence of tunicamycin. The percentage of viable Annexin-V$^-$ cells after 40 h compared to DMSO controls is shown as mean ± s.e.m. of $n = 4$ cord blood samples. $^{**}P < 0.01$, $^{***}P < 0.001$, $^{****}P < 0.0001$.

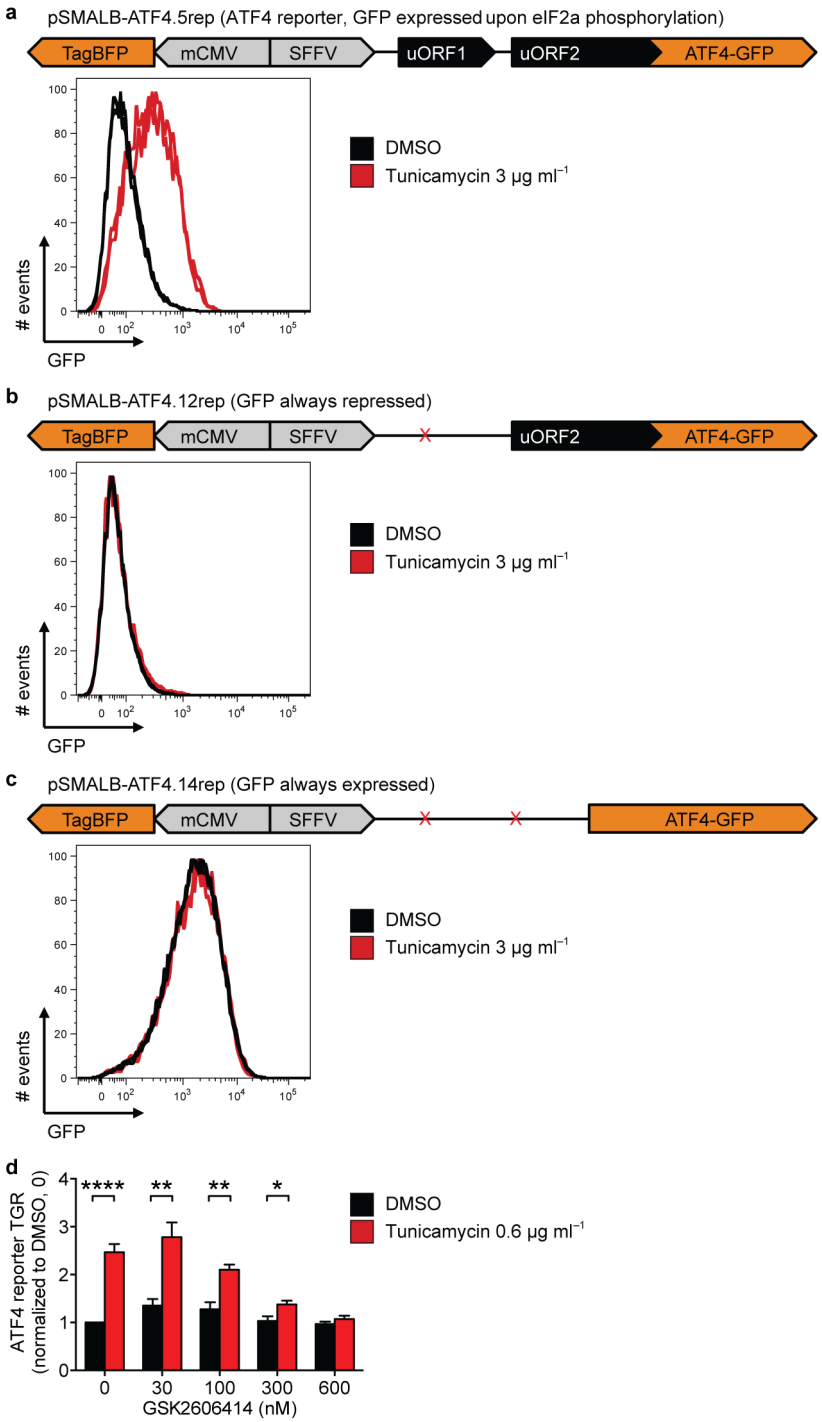

Extended Data Figure 4 | ATF4 reporter enables visualization of increased ATF4 translation after tunicamycin treatment. **a**, ATF4 reporter validation. Two upstream ORFs (uORFs) that are 5′ of the *ATF4* coding sequence in the *ATF4* mRNA ensure more efficient translation of ATF4 when eIF2α phosphorylation levels are high[13,14]. A bidirectional lentiviral vector was constructed that gives constitutive expression of TagBFP to mark transduced cells. In the other direction, the SFFV promoter drives expression of the 5′ end of the *ATF4* mRNA which fuses with a GFP reporter gene 3′ of the termination codon of uORF2. HeLa cells were transduced with pSMALB-ATF4.5rep (referred to as ATF4 reporter) and treated with tunicamycin. After 30 h, GFP fluorescence was read out by flow cytometry. Histogram plots show $n = 2$ technical duplicates (two black lines for DMSO control, two red lines for tunicamycin treatment). **b**, **c**, Reporter fluorescence depends on uORFs. HeLa cells were transduced and treated with tunicamycin. As expected, ATF4–GFP translation is (**b**) repressed in the negative control that has a mutated uORF1 start codon and (**c**) constitutively high in the positive control with mutated start codons for both uORFs[13]. Histogram plots show $n = 2$ technical duplicates. **d**, ATF4 reporter-transduced cord blood cells were treated with tunicamycin and increasing doses of the PERK inhibitor GSK2606414. The transgene ratio (TGR) is shown as mean ± s.e.m. of $n = 6$ cord blood samples (except at 600 nM, $n = 3$ cord blood samples). $^{*}P < 0.05$, $^{**}P < 0.01$, $^{****}P < 0.0001$.

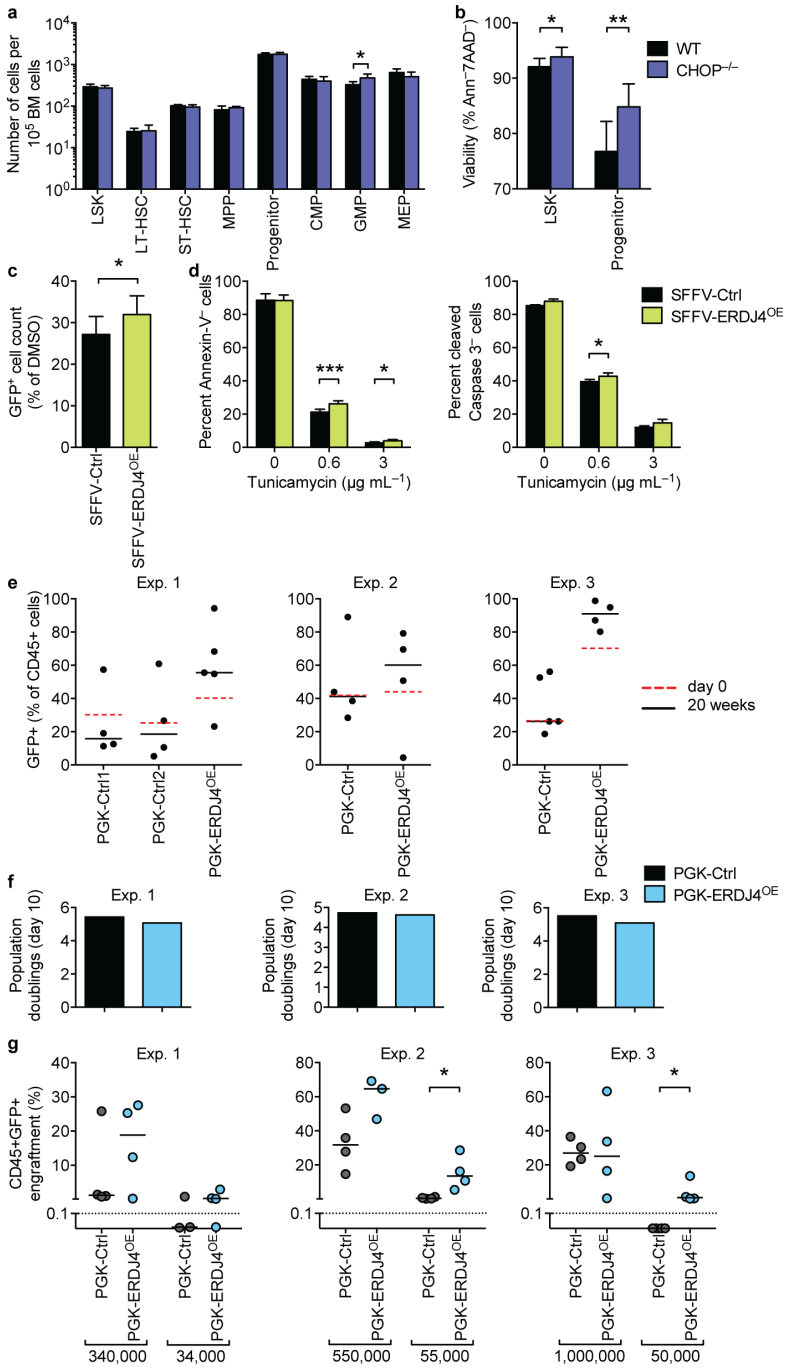

Extended Data Figure 5 | Modulation of UPR-associated genes affects haematopoietic stem and progenitor cells *in vivo*. **a**, Analysis of haematopoietic stem and progenitor cell frequencies in *Chop*$^{-/-}$ mice. Flow cytometry was performed on mouse bone marrow (Extended Data Table 2). Bars show the absolute cell production in each population from wild-type or *Chop*$^{-/-}$ mice. Data are shown as mean ± s.d. of $n = 5$ mice per group. **b**, Viability analysis of stem and progenitor cell populations in *Chop*$^{-/-}$ mice. The percentage of viable Annexin-V$^-$7-AAD$^-$ cells within the HSC-enriched LSK and Lin$^-$Sca-1$^-$c-Kit$^+$ progenitor fractions was assessed by flow cytometry. Data are shown as mean ± s.d. of technical duplicates of $n = 5$ mice per group. **c**, ERDJ4^{OE} cells show increased survival after tunicamycin treatment. The haematopoietic TEX cell line[28] was transduced with SFFV-Ctrl or SFFV-ERDJ4^{OE} lentiviral vectors and plated in the presence of 0.6 μg ml^{-1} tunicamycin (SFFV refers to lentiviral promoter driving transgene expression). After 48 h, the number of transduced cells compared to DMSO-treated controls was determined by automated counting of GFP$^+$ cells. Data are shown as mean ± s.d. of $n = 3$ independent experiments, P value was calculated using a paired t-test. **d**, Tunicamycin-induced apoptosis is reduced by ERDJ4^{OE}. Cells from **c** were analysed for Annexin-V and cleaved caspase-3 expression by flow cytometry. Data are shown as mean ± s.d. of $n = 3$ independent experiments, P values were calculated using paired t-tests. **e**, ERDJ4^{OE} endows cord blood cells with a competitive advantage over untransduced cells. Three cord blood pools (Exp. 1–3) were transduced with PGK-Ctrl or PGK-ERDJ4^{OE} lentiviruses and injected into 5 mice each. Dashed line indicates GFP% after transduction (day 0); solid line indicates median GFP% of the human CD45$^+$ graft in the injected femur of xenografted mice (20 weeks). Every symbol represents one mouse. **f**, Similar expansion of PGK-Ctrl and PGK-ERDJ4^{OE} transduced cord blood cells *in vitro*. Three cord blood pools (Exp. 1–3) were transduced with PGK-Ctrl or PGK-ERDJ4^{OE} lentivirus and expanded for 10 days in liquid culture. Total population doublings of transduced GFP$^+$ cells is shown. **g**, ERDJ4^{OE} increases HSC output. After liquid culture, GFP$^+$ cells from **f** were sorted and injected at high and low cell doses, indicated below the x axis. Total human CD45$^+$GFP$^+$ engraftment in the injected femur after 10 weeks is shown. P values were calculated using the Mann–Whitney U-test. Every symbol represents one mouse, line shows median. $^*P < 0.05$, $^{**}P < 0.01$, $^{***}P < 0.001$.

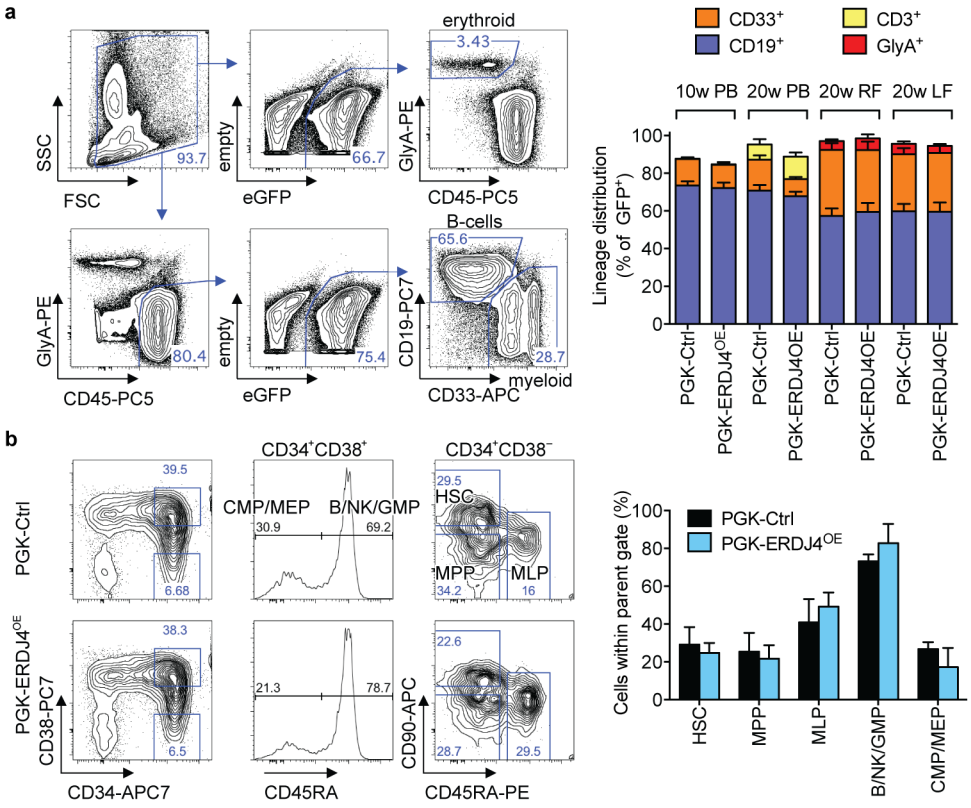

d

	Cell # injected	Engrafted / total mice	HSC frequency 0.95 confidence interval
PGK-Ctrl	1,000,000	7/7 (100%)	
	750,000	2/4 (50%)	
	500,000	1/1 (100%)	Lower: 1 / 886,576
	300,000	0/4 (0%)	Estimate: 1 / 512,185
	250,000	0/3 (0%)	Upper: 1 / 295,895
	200,000	2/4 (50%)	
	100,000	3/5 (60%)	
	30,000	0/3 (0%)	
PGK-ERDJ4^{OE}	1,000,000	7/7 (100%)	
	750,000	3/4 (75%)	
	500,000	2/4 (50%)	Lower: 1 / 669,122
	300,000	2/2 (100%)	Estimate: 1 / 397,687
	250,000	1/3 (33%)	Upper: 1 / 236,362
	200,000	1/4 (25%)	
	100,000	2/5 (40%)	
	30,000	0/3 (0%)	

Extended Data Figure 6 | Lineage differentiation, progenitor cell frequencies, homing, and serial transplantability are maintained following ERDJ4^{OE}. **a**, PGK-ERDJ4^{OE}-transduced cord blood maintains multilineage differentiation potential *in vivo*. Left: gating scheme to assess differentiation of the human graft in mouse bone marrow. Representative flow plots show quantification of CD45$^+$CD19$^+$ B cells, CD45$^+$CD33$^+$ monocytes and granulocytes, and CD45$^-$GlyA$^+$ erythroid cells within the GFP$^+$ graft. Right: the differentiation of transduced cord blood cells was assessed in the peripheral blood (PB) at 10 and 20 weeks and in the injected (RF) and non-injected (LF) femur at 20 weeks after transplantation. Results are shown as mean ± s.e.m. of $n = 15$ mice representing $n = 3$ cord blood samples. **b**, ERDJ4^{OE} does not cause aberrant expansion of stem or progenitor cell fractions. To assess the distribution of human stem and progenitor cells, lineage$^+$ and mouse cells were depleted from xenografted mouse bone marrow. The remaining human lineage$^-$ cells were analysed by flow cytometry. Left: gating scheme to assess differentiation into HSC, MPP, MLP, CMP/MEP and B/NK/GMP fractions (Extended Data Table 1). Right: the frequency of human stem and progenitor cells within the human CD45$^+$GFP$^+$ graft was assessed 20 weeks after transplantation of transduced cord blood cells. Results are shown as mean ± s.e.m. of $n = 3$ cord blood samples. **c**, Homing capacity to the non-injected bone marrow is not altered by ERDJ4^{OE}. Transduced cord blood cells were expanded for 12 days in liquid culture conditions and 1–1.6 × 10^6 cells were transplanted per mouse. After 19 h, mice were euthanized to assess human CD45$^+$GFP$^+$ cell homing to the non-injected femur. Results were normalized to transduction efficiency. Every symbol represents one mouse, results of $n = 3$ cord blood samples are shown with 2 mice per group each; line shows median. **d**, Frequency of functional human HSCs *in vivo* is maintained with ERDJ4^{OE}. Cord blood cells were transduced and injected into primary mice. After 10 weeks, mice were killed and transduced GFP$^+$ cells were sorted from their bone marrow. Thirty thousand to one million cells were re-transplanted into secondary mice for serial LDA. After 10 weeks, the bone marrow of secondary mice was assessed for human CD45$^+$GFP$^+$ engraftment; mice were scored as positive if the engraftment level was >0.01%. Data from $n = 3$ cord blood samples was pooled.

Extended Data Table 1 | Surface marker phenotypes to separate human stem and progenitor cell subsets

Population	Surface phenotype
HSPC	$CD34^+CD38^-$
HSC	$CD34^+CD38^-CD45RA^-CD90^+$
$CD49f^+$ HSC	$CD34^+CD38^-CD45RA^-CD90^+CD49f^+$
MPP	$CD34^+CD38^-CD45RA^-CD90^-$
$CD49f^-$ MPP	$CD34^+CD38^-CD45RA^-CD90^-CD49f^-$
MLP	$CD34^+CD38^-CD45RA^+CD90^{-/lo}$
Progenitor	$CD34^+CD38^+$
CMP/MEP	$CD34^+CD38^+CD45RA^-$
B/NK/GMP	$CD34^+CD38^+CD45RA^+$
CMP	$CD34^+CD38^+CD45RA^-CD10^-CD135^+$
MEP	$CD34^+CD38^+CD45RA^-CD10^-CD135^-$
B/NK	$CD34^+CD38^+CD45RA^+CD10^+$
GMP	$CD34^+CD38^+CD45RA^+CD10^-CD135^+$

HSPC, haematopoietic stem and progenitor cell; HSC, haematopoietic stem cell; MPP, multipotent progenitor; MLP, multilymphoid progenitor; CMP, common myeloid progenitor; MEP, megakaryocyte erythrocyte progenitor; B/NK, B and NK cell progenitor; GMP, granulocyte macrophage progenitor. 'HSPC' to 'HSC' to '$CD49f^+$ HSC' indicates increasing purity of the population: approximately 1:75, 1:20 and 1:10, respectively[7,9].

Extended Data Table 2 | Surface marker phenotypes to separate mouse stem and progenitor cell subsets

Population	Surface phenotype
LSK	$Lin^{-}Sca\text{-}1^{+}c\text{-}Kit^{+}$
LT-HSC	$Lin^{-}Sca\text{-}1^{+}c\text{-}Kit^{+}Flk2^{-}CD34^{-}$
ST-HSC	$Lin^{-}Sca\text{-}1^{+}c\text{-}Kit^{+}Flk2^{-}CD34^{+}$
MPP	$Lin^{-}Sca\text{-}1^{+}c\text{-}Kit^{+}Flk2^{+}CD34^{+}$
Progenitor	$Lin^{-}Sca\text{-}1^{-}c\text{-}Kit^{+}$
CMP	$Lin^{-}Sca\text{-}1^{-}c\text{-}Kit^{+}FcγII/IIIR^{lo}CD34^{+}$
GMP	$Lin^{-}Sca\text{-}1^{-}c\text{-}Kit^{+}FcγII/IIIR^{hi}CD34^{+}$
MEP	$Lin^{-}Sca\text{-}1^{-}c\text{-}Kit^{+}FcγII/IIIR^{-}CD34^{-}$

LSK, HSC-enriched $Lin^{-}Sca\text{-}1^{+}c\text{-}Kit^{+}$ cells; LT-HSC, long-term haematopoietic stem cell; ST-HSC, short-term haematopoietic stem cell; MPP, multipotent progenitor; CMP, common myeloid progenitor; GMP, granulocyte macrophage progenitor; MEP, megakaryocyte erythrocyte progenitor.

Extended Data Table 3 | Primer sequences used for quantitative RT–PCR

Gene	Primer	Sequence 5' to 3'
ACTB	forward	CCTGTACGCCAACACAGTGC
ACTB	reverse	ATACTCCTGCTTGCTGATCC
ATF4	forward	GCTAAGGCGGGCTCCTCCGA
ATF4	reverse	ACCCAACAGGGCATCCAAGTCG
ATF6	forward	ATGAAGTTGTGTCAGAGAACC
ATF6	reverse	CTCTTTAGCAGAAAATCCTAG
CHOP/DDIT3	forward	GGAGCATCAGTCCCCCACTT
CHOP/DDIT3	reverse	TGTGGGATTGAGGGTCACATC
ERDJ4/DNAJB9	forward	TCGGCATCAGAGCGCCAAATCA
ERDJ4/DNAJB9	reverse	ACCACTAGTAAAAGCACTGTGTCCAAG
ERO1LB	forward	TTCTGGATGATTGCTTGTGTGAT
ERO1LB	reverse	GGTCGCTTCAGATTAACCTTGT
GADD34/PPP1R15A	forward	CCCAGAAACCCCTACTCATGATC
GADD34/PPP1R15A	reverse	GCCCAGACAGCCAGGAAAT
GRP78/HSPA5/BiP	forward	TGACATTGAAGACTTCAAAGCT
GRP78/HSPA5/BiP	reverse	CTGCTGTATCCTCTTCACCAGT
GRP94/HSP90B1/TRA1	Qiagen	Qiagen cat. number QT00046963
IRE1/ERN1	forward	TGCTTAAGGACATGGCTACCATCA
IRE1/ERN1	reverse	CTGGAACTGCTGGTGCTGGA
PERK/EIF2AK3	forward	AATGCCTGGGACGTGGTGGC
PERK/EIF2AK3	reverse	TGGTGGTGCTTCGAGCCAGG
PBGD/HMBS	forward	CATGTCTGGTAACGGCAATG
PBGD/HMBS	reverse	GTACGAGGCTTTCAATGTTG
Spliced *XBP1*	forward	CGCTTGGGGATGGATGCCCTG
Spliced *XBP1*	reverse	CCTGCACCTGCTGCGGACT
Total *XBP1*	forward	GGCATCCTGGCTTGCCTCCA
Total *XBP1*	reverse	GCCCCCTCAGCAGGTGTTCC